An Alveolata secretory machinery adapted to parasite host cell invasion

Eleonora Aquilini, Marta Mendonça Cova, Shrawan Kumar Mageswaran, Nicolas dos Santos Pacheco, Daniela Sparvoli, Diana Penarete-Vargas, Rania Najm, Arnault Graindorge, Catherine Suarez, Marjorie Maynadier, et al.

Title:

An Alveolata secretory machinery adapted to parasite-host cell invasion

Authors

Eleonora Aquilini[1§], Marta Mendonça Cova[1§], Shrawan Kumar Mageswaran[2], Nicolas Dos Santos Pacheco[1], Daniela Sparvoli[1,3], Diana Marcela Penarete-Vargas[1], Rania Najm[1], Arnault Graindorge[1], Catherine Suarez[1], Marjorie Maynadier[1], Laurence Berry-Sterkers[1], Serge Urbach[4], Pilar Ruga Fahy[5], Amandine N. Guérin[6], Boris Striepen[6], Jean-François Dubremetz[1], Yi-Wei Chang[2], Aaron P. Turkewitz[3], Maryse Lebrun[1*]

Affiliations

[1]UMR 5235 CNRS, Université de Montpellier, 34095 Montpellier, France

[2]Department of Biochemistry and Biophysics, University of Pennsylvania, Philadelphia, USA

[3]Department of Molecular Genetics and Cell Biology, University of Chicago, Chicago, USA

[4] IGF, Université de Montpellier, CNRS, INSERM, 34000 Montpellier, France

[5]Pôle Facultaire de Microscopie Ultrastructurale, CH-1211 Geneva, Switzerland

[6]Department of Pathobiology, School of Veterinary Medicine, University of Pennsylvania, Philadelphia, PA 19104, USA

[§]These authors contributed equally to the work

*Corresponding author

Manuscript Text: 2499 words

Apicomplexa are unicellular eukaryotes and obligate intracellular parasites, including *Plasmodium*, the causative agent of malaria and *Toxoplasma*, one of the most widespread zoonotic pathogens. Rhoptries, one of their specialized secretory organelles, undergo regulated exocytosis during invasion[1]. Rhoptry proteins are injected directly into the host cell to support invasion and subversion of host immune function[2]. The mechanism by which they are discharged is unclear and appears distinct from those in bacteria, yeast, animals or plants. Here we show that rhoptry secretion in Apicomplexa shares structural and genetic elements with the exocytic machinery of ciliates, their free-living relatives. Rhoptry exocytosis depends on intramembranous particles in the shape of a rosette embedded into the plasma membrane of the parasite apex. Formation of this rosette requires multiple Non-discharge (Nd) proteins conserved and restricted to Ciliata, Dinoflagellata, and Apicomplexa, that together constitute the superphylum Alveolata. We identified Nd6 at the site of exocytosis in association with an apical vesicle. Sandwiched between the rosette and the tip of the rhoptry, this vesicle appears as a central element of the rhoptry secretion machine. Our results describe a conserved secretion system that was adapted to provide defense for free-living unicellular eukaryotes and host cell injection in intracellular parasites.

Apicomplexan parasites are invasive and defined by the presence of an apical complex used to recognize and gain entry into host cells. It includes two secretory organelles: micronemes and rhoptries[3]. Microneme proteins are secreted to the parasite surface and mediate motility, host cell recognition and invasion[4]. Rhoptry proteins are injected directly into the host cell[2], where they anchor the machinery propelling the parasite into the host cell[5], facilitate nutrient

import[6–8], interfere with the immune response, and modulate gene expression to promote infection[9]. Rhoptry secretion requires a trigger in the form of microneme proteins binding to host cell receptors[10,11]. Importantly, rhoptry proteins not only cross the plasma membrane of the parasite (exocytosis) but also that of the host[1,12]. Rhoptry exocytosis factors identified to date[11,13,14] are mostly specific to Apicomplexa, suggesting that these cells depend on unique lineage-restricted secretory mechanisms. Consistent with this, no eukaryotic SNAREs, the main drivers for fusing vesicles to target membrane in eukaryotic system, have so far been associated with rhoptry exocytosis. Apicomplexa also lack genes encoding prokaryotic secretion systems[15]. Thus, how rhoptry effectors are delivered into the host cytoplasm remains unclear.

To explore the mechanisms of rhoptry secretion, we searched for examples of regulated secretion in organisms phylogenetically closely related to Apicomplexa[16]. All Alveolata bear alveolar sacs beneath the plasma membrane, which give the superphylum its name. They contain elaborate membrane-bounded secretory organelles with shared evolutionary origin[6] but different morphologies and functions. Known as trichocysts in the Ciliata *Paramecium*, they function in defense—docking at the plasma membrane and discharging in response to predation[17]. Exocytic membrane fusion occurs at plasma membrane sites consisting of rosettes of 8-9 intramembranous particles (IMPs)[18,19]. Previous electron microscopy (EM) studies have described similar rosettes at the apex of several apicomplexan parasites[20–23]. Though suggested to be involved in exocytic fusion[20], the function of the IMPs rosette has never been experimentally addressed in Apicomplexa. Analysis of *Paramecium tetraurelia* mutants defective in both trichocyst exocytosis and rosette assembly[24,25] led to identification of *nd* (non-discharge) genes[26–29] (Supplementary Table 1). To determine if similar factors could be involved in exocytosis of secretory organelles in Apicomplexa, we first searched for Nd homologs in the tree of life. Genome

mining for *nd* genes and phylogenetic analyses revealed that *nd6* and *nd9* are conserved in Ciliata, but also in Dinoflagellata, Chromerida and Apicomplexa (Extended data Fig. 1 and Extended Data 1). We also found Nd9 homolog in the Perkinsozoa, a sister group of Dinoflagellata. Altogether, this analysis suggested a conserved evolution and common function of *nd* genes across Alveolata.

To define the parasite localization of Nd proteins, we tagged *nd6* (TGGT1_248640) and *nd9* (TGGT1_249730) at the endogenous loci in *Toxoplasma gondii*, an experimentally tractable apicomplexan (Extended data Fig. 2). Both proteins displayed a punctuate signal throughout the cytoplasm, but in addition *Tg*Nd6 accumulated at the apical tip of the parasite (Fig. 1a, b). A closer look at the apical tip by immuno- EM localized *Tg*Nd6 at the site of rhoptry exocytosis, in association with the parasite plasma membrane and an underlying membranous spheroid known as the "apical vesicle (AV)" (Fig. 1c). Despite previously observed by EM in *Toxoplasma*[21,30] and suggested to be linked to rhoptries[22,30], the composition and function of the AV remain unknown.

Because *Tg*Nd6 and *Tg*Nd9 were predicted to be fitness-conferring genes[31], in order to investigate their function we generated inducible knockdown mutants using an auxin-inducible degron for *Tg*Nd6[32] and tetracycline-induced repression for *Tg*Nd9[33,34] (Extended data Fig. 2). Parasites conditionally depleted of *Tg*Nd6 or *Tg*Nd9 showed reduced plaque formation on fibroblast monolayers, indicating the inability of both mutants to efficiently complete the lytic cycle (Extended Data Fig. 3a). *Tgnd6*-iKD and *Tgnd9*-iKD mutants showed no detectible defects in their intracellular replication, egress, conoid protrusion, motility, or host cell attachment (Extended Data Fig. 3b-g). In contrast, invasion was severely impaired for both mutants (Fig. 1d).

To understand the mechanistic basis of this invasion defect, we evaluated microneme and rhoptry secretion in the *Tgnd6*-iKD and *Tgnd9*-iKD mutants. Release of the micronemal

protein AMA1 into the supernatant was unimpeded by the absence of *Tg*Nd6 or *Tg*Nd9 (Fig. 1e). In contrast, rhoptry secretion was significantly impaired by the loss of *Tg*Nd6 or *Tg*Nd9 as revealed by quantifying the release of rhoptry protein ROP1 into host cells using immunofluorescence assays (IFA)[35] (Extended Data Fig. 3h), or the delivery of Cre recombinase fused to the rhoptry protein toxofilin into the nucleus of a suitable reporter cell[36] (Fig. 1f). This was not due to defects in rhoptry biogenesis, as the mutants showed normal organelle formation and apical positioning, as judged by IFA and EM (Extended Data Fig. 4). Analysis by freeze fracture EM of the apex of *TgNd6*-iKD mutants showed no significant reduction in the presence of the apical rosette (Fig. 1g). In contrast, *T. gondii* depleted of *Tg*Nd9 displayed a strong decrease in cells with a rosette at the parasite apex (Fig. 1g). This last result link rosette formation with rhoptry secretion and support an evolutionarily conserved mechanism of regulated exocytosis in Alveolata.

To determine whether other Apicomplexa require *nd* genes for rhoptry function, we analysed Nd9 in *Plasmodium falciparum*, the causative agent of the deadliest form of malaria. We confirmed that *P. falciparum* intracellular merozoites possess a fusion rosette of 8 IMPs (Fig. 2a). As *nd9* is also predicted to have a fitness cost in *P. falciparum*[36], we used the rapamycin-inducible dimerizable Cre recombinase (DiCre) system[37] to conditionally excise the low expressed *Pfnd9* gene (PF3D7_1232700) (Extended Data Fig. 5a-d). DiCre mediated ablation of *Pfnd9* resulted in substantial reduction in parasite proliferation (Fig. 2b), which was due to the inability of *Pfnd9*-iKO mutants to reinvade host cells while their intracellular development and egress were unaffected (Fig. 2b, c; Extended Data Fig. 5e). As in *T. gondii*, microneme secretion was unaltered in *Pfnd9*-iKO parasites (Fig. 2d) but rhoptry secretion was affected (Fig. 2e).

To gain a more complete understanding of the molecular composition of the rhoptry secretion machinery, we searched for Nd interacting proteins in *T. gondii*. *Tg*Nd9 displays

two Armadillo repeats while *Tg*Nd6 shows homology with GDP/GTP exchange factors (GEFs) known to activate GTPases (Fig. 3a). We used *Tg*Nd9 for immunoprecipitation (IP) experiments as we found *Tg*Nd6 to be largely insoluble (Extended data Fig. 2g). Mass spectrometry analysis revealed robust interaction of *Tg*Nd9 with *Tg*Nd6 and with *Tg*FER2 (TGGT1_260470), a member of the ferlin calcium sensor family, known to be essential for *Toxoplasma* rhoptry secretion[13] (Fig. 3a and Supplementary Table 2). The *Tg*Nd9 IP also enriched TGGT1_222660, a protein harboring Armadillo repeats and Leucine Rich Repeats, named hereafter *Tg*NdP1 (Nd Partner 1) and TGGT1_316730 (*Tg*NdP2: Nd Partner 2), a protein with a C2 calcium lipid binding domain (Fig. 3a). Both genes are broadly shared among Alveolata (Extended Data Fig. 1c, d and Supplementary Data 1) and predicted to be fitness-conferring in *Toxoplasma*[31] and *Plasmodium*[38]. In contrast, *Tg*Nd9-IP interactor TGGT1_277840, a GTPase, is restricted to Apicomplexa and Dinoflagellata, and TGGT1_253570 is only found in the apicomplexan subgroup Coccidia. Importantly, all these proteins are also recovered when using reverse IP with tagged-*Tg*NdP1 protein (Supplementary Table 3).

To learn more about the new conserved partners of *Tg*Nd9, we generated *T. gondii* lines in which *Tg*NdP1 or *Tg*NdP2 was tagged by an epitope and could be ablated conditionally (Extended Data Fig. 6). Both proteins appear as punctate cytoplasmic staining (Fig. 3b) but *Tg*NdP2—like *Tg*Nd6—also appears as a dot at the apical tip of the parasite, although consistently with lower intensity. Depletion of *Tg*NdP1 or *Tg*NdP2 resulted in a profound growth defect (Extended Data Fig. 7a) that we linked to impairment of host cell invasion and rhoptry secretion (Fig. 3c, d and Extended Data Fig. 7). Again, loss of rhoptry secretion went hand-in-hand with loss of the rosette in *Tgndp1*-iKD and *Tgndp2*-iKD parasites (Fig. 3e).

To further validate our conservation data and broaden our discoveries back to Ciliata, we generated knockouts for orthologues of both NdP1 (TTHERM_01287970, *Ttn*Δ*ndp1*) and NdP2 (TTHERM_00498010; *Ttn*Δ*ndp2*) in the free-living Ciliata *Tetrahymena thermophila* (Extended Data Fig. 8a, b). The homologous organelles to *Paramecium* trichocysts in *Tetrahymena* are called mucocysts and are non-essential for laboratory growth. We found that *Ttn*Δ*ndp1* and *Ttn*Δ*ndp2* cells were defective in mucocyst secretion, which was triggered by exposure to dibucaine[39] (Fig. 3f). We further showed that the impairment of exocytosis was not due to defects in mucocyst biogenesis, given that mucocyst maturation (as measured by processing of mucocyst pro-proteins) and trafficking (monitored by IFA) remained unaltered (Extended Data Fig. 8c, d). Taken together, we identified a complex of proteins essential for organellar exocytosis and rosette assembly, conserved across Alveolata.

The exact position of the rosette relative to the apical tip of the rhoptry and the enigmatic AV remained elusive, since freeze-fracture technique—used to image the rosette on the membrane—does not capture the internal structures at the same time. To overcome this limitation, we imaged the *Toxoplasma* apex by cryo-electron tomography (cryo-ET)—a technique combining the advantages of 3D imaging with molecular resolution to reveal ultrastructure *in situ* in its native biological context. We were able to simultaneously visualize and define three linked elements — 1) the rosette (dark blue), 2) the AV (magenta), and 3) the apical tip (cyan) of the rhoptry (orange) (Fig. 4a and b, Extended Fig. 9). The rosette showed an 8-fold rotational symmetry around a central axis (Fig. 4c and d) and extended under the parasite plasma membrane (light blue) to interact with the AV (Fig. 4c). Thus, the rosette is tightly sandwiched between the AV and the plasma membrane and extensively interacts with both membranes. The AV in turn sits over the rhoptry tip (Fig. 4a and b). The contiguity of all elements from the rhoptry tip to the plasma membrane supports the idea that the rosette and the AV are integral part of the rhoptry secretion machinery. Interestingly, the

connection between AV and rosette is sometimes observed even in the absence of a docked rhoptry (Fig. 4e) suggesting that they assemble independently of rhoptry docking. Supporting this hypothesis, when we imaged the *Toxoplasma* ARO mutant in which rhoptries fail to dock and are dispersed in the cytoplasm[40], both the rosette (seen by freeze-fracture; Fig. 4f) and the AV (seen by EM; Fig. 4g) were still present at the apex of the parasite. Altogether, these results positioned the rosette and AV at the heart of the exocytic machinery in Apicomplexa and implied that rhoptries do not make contact and fuse directly with the plasma membrane.

Our work breaks ground on the molecular and structural mechanisms for rhoptry exocytosis in Apicomplexa. We defined the apical rosette of IMPs as the site for rhoptry exocytosis in Apicomplexa, and we characterized an Alveolata-specific Nd complex necessary for the assembly of the rosette. In *Paramecium*, physiological studies predicted *Pt*Nd6 to be active at the plasma membrane[24] while *Pt*Nd9 appeared to be a diffusible cytoplasmic component interacting with both trichocyst and plasma membranes[41,42]. However, both the localization and identity of partners in Ciliata remained unknown. We localized *Tg*Nd9 to the cytoplasm and *Tg*Nd6 to the site of exocytosis in *Toxoplasma*. We found both proteins to form a complex that included *Tg*NdP1 and *Tg*NdP2, which we demonstrated to be essential for organelle exocytosis in both Ciliata and Apicomplexa. This complex further includes proteins with C2 domains (*Tg*FER2 and *Tg*NdP2), a homolog of the membrane fusion Ferlin family (FER2)[13], a GTPase (TGME49_277840), and a putative GEF protein (*Tg*Nd6). These proteins and their domains yield a regulatory model in which calcium signaling and nucleotide binding and hydrolysis constitute key steps that control rosette assembly and/or organelle discharge (more discussion in Supplementary text).

In this study, we also shed new light on the enigmatic AV. Described in *Toxoplasma*[22,30], it is also visible in early micrographs from other apicomplexan parasites[20,43,44] (Extended Data Fig. 10). We show that the AV is on one side tightly

connected with the plasma membrane via the rosette, and from the other sits on the tip of the rhoptry, precluding a direct link and fusion between the rhoptry and the plasma membrane. In Ciliata, where no comparable AV is present, the docking and fusion of the trichocysts to the plasma membrane shapes the rosette. Diverging from this scenario, we also showed that the docking of the rhoptries in *Toxoplasma* is dispensable for rosette formation (Fig. 4e-g), which suggests that the assembly of the rosette in *Toxoplasma* might be instead induced by docking of the AV.

While *Paramecium* trichocysts are discharged into the environment to thwart predators, apicomplexan rhoptries translocate their contents directly into the cytoplasm of host organisms to infect and parasitize. The difference in terms of presence or absence of the AV (Fig. 4h) suggests that the AV is an adaptation in Apicomplexa for parasitism and cell invasion. Its presence may reflect additional complexity of the secretory machinery in apicomplexans, in which exocytosis must be coupled with injection of rhoptry content through the barrier of a host cell membrane. In support of this hypothesis, a similar vesicle is present at the apex of *Perkinsus marinus* (previously named *Dermocystidium marinum*)[45]. This organism possesses rhoptries and invades and parasitizes the cells of oysters. Phylogenetically, *Perkinsus* falls between Dinoflagellata and Apicomplexa and is viewed as a basal taxon and example of early adaptation to parasitism.

The rosette and the set of Nd proteins highlight a common ancestry for the fusion machinery linked to secretory organelles in two groups of protists that diverged hundreds of millions of years ago and have adopted radically different lifestyles. The architecture and molecular composition of the rhoptry system that enables the intracellular parasitism of Apicomplexa is now revealed. Future studies combining high resolution structural biology approaches with the genetics and cell biology of *Toxoplasma* will allow a full understanding

of how this fascinating mechanism unfolds and is regulated. Such an understanding may find application in designing strategies against malaria, cryptosporidiosis and toxoplasmosis.

Methods

Parasite Immunofluorescence microscopy

Immunofluorescence assays (IFAs) on intracellular *T. gondii* parasites were conducted as previously described[46]. Briefly, cell monolayers were washed and fixed in 4% paraformaldehyde (PFA) in Phosphate Saline Buffer (PBS) for 20 min. After three washes with PBS, cells were permeabilized with 0.1% (v/v) Triton X-100 or with saponin 0.1% (v/v) (for invading parasites) in PBS for 5 min, blocked with 10% fetal bovine serum in PBS (PFBS) for 45 min, incubated with primary Abs diluted in 2% PFBS, washed three times, and then incubated with secondary antibody. The coverslips were mounted onto microscope slides using Immunomount (Calbiochem).

For IFAs on *P. falciparum*, thin blood smears of highly synchronized DMSO and rapamycin-treated *PfNd9*-iKO schizonts were air-dried, fixed in 4% (w/v) PFA and permeabilized in 0.1% (v/v) Triton X-100. After blocking in 1.5% BSA, samples were probed for 1 h with the suitable antibodies: rabbit anti-*Pf*AMA1[47] antibody (1:1000); mouse anti-*Pf*MSP1[48] antibody (1:1000); mouse anti-*Pf*RAP2[49] antibodies (1:500). The secondary antibodies used were Alexa Fluor 488 and 594-conjugated antibodies against mouse or rabbit IgG (highly cross-adsorbed) both diluted 1:4000 (Molecular Probes). Samples were then counterstained with Hoechst and slides mounted with Vectashield® antifade mounting medium.

Except when specified, observations were performed with a Zeiss Axioimager Z1 epifluorescence microscope equipped with a Zeiss Axiocam MRm CCD camera and 100X/1.4 Oil Plan Apochromat objective. Images were processed using Zen Blue 2.3 pro

(Zeiss) software. Imaging of *Tg*Nd6, *Tg*Nd9, *Tg*NdP1 and *Tg*NdP2 co-localization with rhoptry protein *Tg*ARO (Fig. 1 and Fig. 3) was performed on a ZEISS confocal LSM880, equipped with an Airyscan detector and a 63X/1.4 Oil Plan Apochromat objective. Zen Black (Zeiss) was used for image airyscan processing. Z-stack images and z-projection images were denoised, adjusted in brightness and contrast, and colored with the program Fiji[50].

Adjustments for brightness and contrast were applied uniformly on the entire images and when required, matching pairs of images were recorded with the same exposure time and processed identically. All optical images were collected at the Montpellier Ressources Imagerie facility of the University of Montpellier (MRI, www.mri.cnrs.fr).

Invasion assays

Toxoplasma plaque assays, replication assays, and two-color invasion assays were performed as previously described[35,51]. Briefly, to synchronize invasion, freshly egressed tachyzoites (5 × 10^6), pre-treated for 48 h ± ATc (*Tgnd9*-iKD and *Tgndp1*-iKD) or 24 h ± IAA (*Tgnd6*-iKD and *Tgndp2*-iKD), were harvested and settled on ice for 20 min on HFF monolayer grown on coverslips in 24-well plates. Invasion was allowed for 5 min at 38 °C and stopped by fixation with 4% PFA in Hank's Balanced Salt Solution (HBSS) for 20 min at room temperature. To detect extracellular parasites, immuno-detection was performed with the mouse mAb T4 1E5 anti-SAG1 antibody (dilution 1:1000) in 2% FCS/HBSS, without previous permeabilization. After permeabilization with 0.01% saponin for 15 min, a second IFA was performed using rabbit anti-ROP1 antibody (dilution 1:1000) to label the parasitophorous vacuole of intracellular parasites. Extracellular and intracellular parasites were counted by microscopic examination of at least 20 fields per coverslip (n=3 coverslips). Graphs show the mean of three independent invasion assays.

Microneme secretion assay

Microneme secretion in *T. gondii* was assayed by monitoring the release into the culture medium. Freshly egressed *T. gondii* tachyzoites, pre-treated for 48 h ± ATc (*Tgnd9*-iKD and *Tgndp1*-iKD) or 24 h ± IAA (*Tgnd6*-iKD and *Tgndp2*-iKD), were harvested by centrifugation at 600 g, and washed twice in intracellular buffer (5 mM NaCl, 142 mM KCl, 1 mM $MgCl_2$, 2 mM EGTA, 5.6 mM glucose and 25 mM HEPES, pH 7.2), prewarmed to 37°C. Parasites were resuspended in DMEM (supplemented with 2 mM glutamine) ± propranolol 500 µM, and incubated at 37°C for 20 min to induce microneme secretion. Parasites were pelleted at 1000 g for 5 min at 4°C, washed once in PBS and stored at -20°C. Supernatants were centrifuged at 2000 g for 5 min, at 4°C and used as ESA (excreted/secreted antigen). Pellets and ESA samples were analysed for micronemal protein (AMA1) by Western blot.
Microneme secretion in *P. falciparum* was assayed by monitoring the surface translocation of AMA1. Highly synchronized DMSO and rapamycin-treated *Pfnd9*-iKO schizonts were exposed to 10 µM E64 to block egress. IFAs were then performed with anti-*Pf*AMA1 antibodies to analyse AMA1 translocation to the merozoite surface.

Rhoptry secretion assays

To evaluate the efficiency of rhoptry secretion in *T. gondii*, we expressed in the *Tgnd*-iKD and *Tgndp*-iKD lines a rhoptry secretion reporter protein consisting of the rhoptry protein toxofilin fused with Cre-recombinase, a nuclear localization signal (NLS), and a myc tag, collectively called Secreted Cre, Epitope-tagged (SeCrEt)[36]. The reporter strains generated were called *Tgnd9*-iKD_SeCrEtUPRT, *Tgndp1*-iKD_SeCrEtUPRT, and *Tgnd6*-iKD_SeCrEtHXGPRT. Ds Red cells, constitutively expressing DsRed and able to switch to eGFP expression upon Cre-mediated recombination, were used as reporter cells[36]. DsRed

Cells were maintained at < 50% confluence (regardless of the flask size) and plated the day before parasite infection, at a density of 2 x 10^5 cells /ml (in T25 flasks). Tachyzoites pre-treated for 48 h ± ATc (*Tgnd9*-iKD and *Tgndp1*-iKD) or 24 h ± IAA (*Tgnd6*-iKD) were collected and used to infect the DsRed cells at a multiplicity of infection (MOI) of 3. 24 hours post-invasion (hpi) infected DsRed cells were trypsinized and examined by fluorescence-activated cell sorting (FACS) to assess the percentage of Ds-Red (rhoptry secretion impairment) and GFP (successful rhoptry secretion) expressing cells. Number of GFP positive cells were normalized as the percentage compared to 100% in the control (-IAA or -ATc).

Additionally, rhoptry secretion has been also quantified by classical e-vacuole assay[35]. Freshly egressed parasites, pre-treated for 48 h ± ATc (*Tgnd9*-iKD and *Tgndp1*-iKD) or 24 h ± IAA (*Tgnd6*-iKD), were preincubated with 1 µM of cytochalasin D (cytD) for 10 min and then incubated with HFF cells in the presence of cytD for 15 min. IFAs were then performed with anti-ROP1 (rhoptry secretion) and anti-SAG1 (parasite surface), and the number of ROP1 stainings per field was determined by microscopic examination of at least 20 fields per coverslip (n = 3 coverslips).

To quantify rhoptry secretion in *P. falciparum,* the same amount of DMSO and rapamycin-treated *Pfnd9*-iKO purified schizonts were arrested with 1.5 µM C2 for 4 h before being washed twice in order to allow them to egress. Parasites were then incubated for 30 min in complete medium with 1 µM cytD in the presence of red blood cells (RBCs). IFAs were then performed with anti-*Pf*RAP2 antibodies to visualise rhoptry secretion events ('spits' of RAP2 export into the RBC). The number of secretion events were counted over the total of RBCs by microscopic examination of 11 fields (~3000 events analysed).

Freeze-fracture

Cells used for the freeze-fracture were harvested, pelleted and fixed in 2.5% glutaraldehyde in 0.1 M phosphate buffer at room temperature for 2 h. Following primary fixation, the samples were rinsed in the same buffer, and kept overnight in 30% glycerol 0.1 M phosphate solution. The cells were then quickly frozen by immersion in liquid nitrogen under vacuum. The frozen samples were fractured in a BAL-TEC BAF 060 apparatus; subsequently the fracture face was shadowed by evaporating platinum 45° (3.2nm) and Carbon 90° (25nm). The replicas were then washed in 6.5% sodium hypochlorite, rinsed in a chloroform (2/3) - (1/3) solution, rinsed in distilled water and mounted on copper grids. In order to interpret the replicas obtained in freeze-fracture technique one must keep in mind that the portion of the lipid bilayer associated with the exterior of the cell is termed the E-face, or extracellular face. The portion associated with the interior of the cell is termed the P-face, or protoplasmic face[52].

In vitro growth assay of _P. falciparum_ parasite asexual development

The growth capability of *Pfnd9*-iKO mutant parasites was assessed by comparing it with the *p230p* DiCre parental line[53] ± rapamycin in biological triplicates. DMSO (vehicle control) and rapamycin-treated cultures were synchronized at ring stages by sorbitol synchronization and parasitaemia adjusted to 0.2% to follow growth over 3 cycles. Parasites around 30 hpi were collected at each cycle to determine parasitaemia by counting Giemsa-stained parasites on at least 1000 RBCs per culture.

P. falciparum induced egress and time-lapse microscopy

P. falciparum egress was imaged using C2 compound to tightly synchronize egress. DMSO and rapamycin-treated *Pfnd9-i*KO parasites were highly synchronized and blocked 40 hpi (mature schizonts) with 1.5 µM C2 compound to prevent egress. Four hours later parasites

were washed twice with warm RPMI 1640 medium (Gibco), to remove C2, and placed into a 35 mm Dish (MatTek). The parasites suspension was sealed by adhering a 22 x 22 mm square coverslip to the Dish and the preparation was introduced on a temperature-controlled microscope stage at 37°C. Bright field images were collected 5 min after washing off the C2 at 1 s intervals over a total of 15 min using a ZEISS AxioObserver Microscope fitted with a coolsnap HQ2 digital camera and 63X/1.4 Oil Plan Apochromat objective. Images were exported to MOV movies using ZEN 2 (blue edition) software. Number of egress events in 15 min were normalized as the percentage compared to 100% in the control.

***Tetrahymena* dibucaine assay to quantify mucocyst secretion**

Tetrahymena cells were grown to stationary phase (10^6 cells/ml) in 25 ml SPP (2% proteose peptone, 0.1% yeast extract, 0.2% dextrose and 0.003% ferric-EDTA supplemented with 250 µg/ml penicillin G, 250 µg/ml streptomycin sulfate, and 0.25 µg/ml amphotericin B fungizone) for 48 h, and then concentrated by centrifugation into a lose 1.5ml pellet. Cells were stimulated with 2.5 mM dibucaine, vigorously mixed for 30 s and diluted to 15 ml with 10 mM Hepes, pH 7.5, and 5 mM CaCl2. After gently mixing, the culture was centrifuged at 1,200 g for 2 min, resulting in the formation of a cell pellet/flocculent bilayer. Quantification of mucocysts secretion has been done by weighing the flocculent layer overlying the pellet of cells.

Transmission electron microscopy

Tgnd9-iKD and *Tg*ARO-iKD, together with the *Δku80*-TATi parental strain, were treated with ATc for 72 h. *Tgnd6*-iKD parasites, and *Δku80*-Tir1 parental strain were treated with IAA for 24 h. Extracellular parasites were collected in the culture medium after natural egress and fixed by adding and equal volume of phosphate buffer 0.1 M containing 5% of

glutaraldehyde for one hour at RT. Parasites were then centrifuged and resuspended in 1 ml of fresh buffer with 2.5% glutaraldehyde for 2 h before being kept at 4°C until further processing. Each of the following steps were performed in suspension followed by centrifugation steps in a tabletop microcentrifuge. Sample were post-fixed with 1% OsO_4 and 1.5% potassium ferricyanide in 0.1 M phosphate buffer for 1 hour at RT, washed in water and then incubated in 2% uranyl acetate in water overnight at 4°C. Tachyzoites were then dehydrated in growing concentration of acetonitrile, followed by impregnation in Epon118: acetonitrile 50:50 for 2 hours, 90:10 for 2 additional hours and then overnight in pure epon. Pellets were polymerized in fresh Epon for 48 h at 60°C. 70 nm ultrathin sections were cut with a Leica ultracut (Leica microsystems), counterstained with uranyl acetate and lead citrate.

Immunoelectron microscopy

Tgnd6-HA_3 parasites, infected fibroblast monolayers were trypsinized and fixed with equal volume of 8% formaldehyde (FA) in phosphate buffer overnight at 4°C and resuspended in 4% fresh FA until further processing. Cells were then incubated with 0.1 % glycine in phosphate buffer, pelleted and embedded in 12% gelatin, cut in small blocks (< 1 mm) and infused in 2.3 M sucrose on a rotating wheel for 24 h at 4°C. Gelatin blocks were mounted on specimen pins and frozen in liquid nitrogen. Cryo-sectioning was performed on a Leica UC7 cryo-ultramicrotome, 70 nm cryosections were picked-up in a 1:1 mixture of 2.3 M sucrose and 2% methylcellulose in water and stored at 4°C. For on-grid immunodetection, grids were floated on 2% gelatin in PBS for 30 min at 37°C to remove methylcellulose/sucrose mixture, then blocked with 1% skin-fish gelatin (SFG, Sigma) in PBS for 5 min. Successive immunolabeling steps were performed on drops as follows: 1) rat monoclonal anti-HA antibodies (clone 3F10, Roche) in 1% BSA, 2) rabbit polyclonal anti-rat IgG antibody

(Sigma) in 1% BSA, 3) Protein A-gold (UMC Utrecht) in 1% BSA. Four washes (2 min each) with 0.1% BSA were performed between steps. After Protein A treatment, grids were washed four times for 2 min each with PBS, fixed 5 min in 1% glutaraldehyde in water, and washed six times for 2 min each with distilled water. Grids were then incubated with 2% methylcellulose: 4% uranyl acetate 9:1 on ice in the dark for 15 min, picked-up on a wire loop and air-dried.

All chemicals were from Electron Microscopy Sciences (USA), solvents were from Sigma. Observations and image acquisition were performed on a Jeol 1200 EXII transmission electron microscope at the Electron Microscopy Platform of the University of Montpellier (MEA; http://mea.edu.umontpellier.fr). Transmission electron microscopy images were processed with Fiji for contrast optimization and the Image J plugin was used to make the EM panels.

Cryo-electron-tomography (Cryo-ET)

Freshly isolated *Toxoplasma gondii* cells were suspended in HBSS along with fiducials (10 nm colloidal gold from Ted Pella for alignment of tilt series). A 4 µl drop of the suspension was applied onto EM grids, excess liquid blotted away, and plunge frozen in a liquid ethane/propane mixture (pre-cooled using liquid nitrogen) using a EM GP2 automatic plunger (Leica Microsystems, Wetzlar, Germany)[54]. The blotting chamber was set to 95-100% relative humidity at 37°C and blotting was done either from the sample side of the grid or from the back using Whatman filter paper #1. Plunge-frozen grids were subsequently loaded into autogrid cartridges (ThermoFisher). EM cartridges containing frozen grids were stored in liquid nitrogen and maintained at ≤−170°C throughout storage, transfer and cryo-ET imaging.

Cryo-ET data collection was performed on a ThermoFisher Krios G3i 300 keV field emission gun cryo-TEM equipped with a 6k x 4k K3 direct electron detector (Gatan, Inc.) at the Beckman Center for Cryo-Electron Microscopy in the Singh Center for Nanotechnology, University of Pennsylvania. The camera was operated in electron counting mode to enable motion correction. An energy filter (Gatan Imaging Filter, Gatan, Inc.) with a slit width of 20 eV was used to increase the contrast of the projection images. Additionally, a Volta phase plate was used to boost the image contrast at defoci of negative 2-3 µm. A magnification of 33,000X with corresponding pixel sizes of 2.65 Å was used for imaging. SerialEM software[55] was used for all imaging. Cells were first assessed at lower magnifications for suitability of ice thickness and outer membrane integrity (the parasites sometimes tend to vesiculate their outer membrane possibly in response to blotting). Once the target cells were identified and marked, anchor maps were used to revisit these locations and collect tilt-series in an automated fashion. Each tilt-series was collected from negative 60° to positive 60° with an increment of 2° in an automated fashion using the low dose functions of tracking and focusing. The cumulative dose of each tilt-series ranged between 100 and 150 $e^-/Å^2$. Once acquired, tilt-series were binned twice or four times before aligned using the 10 nm colloidal gold as fiducials and reconstructed into tomograms by our in-house automated computation pipeline utilizing the IMOD software package[56].. For presentation purposes, tomograms were favorably oriented in three dimensions before averaging a few slices around the slice of interest (to enhance contrast) using the slicer window in IMOD. In a few cases (Figs. 4b-e, contrast was further enhanced using the non-linear anisotropic diffusion filter in IMOD.

Immunopurification and mass spectrometry analysis

Immunopurification was performed using anti HA magnetic beads (Pierce R88836) as previously described[57]. Purified proteins were loaded on a SDS-PAGE and digested in gel (2

bands per sample) as previously described[58]. Samples were loaded onto a 25 cm reversed phase column (75 mm inner diameter, Acclaim Pepmap 100® C18, Thermo Fisher Scientific) and separated with an Ultimate 3000 RSLC system (Thermo Fisher Scientific) coupled to a Q Exactive HFX (Thermo Fisher Scientific). MS/MS analyses were performed in a data-dependent mode. Full scans (375 – 1,500 m/z) were acquired in the Orbitrap mass analyzer with a resolution of 60,000 at 200 m/z. For the full scans, 3e6 ions were accumulated within a maximum injection time of 60 ms. The twelve most intense ions with charge states ≥ 2 were sequentially isolated (1e5) with a maximum injection time of 45 ms and fragmented by HCD (Higher-energy collisional dissociation) in the collision cell (normalized collision energy of 28%) and detected in the Orbitrap analyzer at a resolution of 30,000.

Raw spectra were processed using the MaxQuant[59] using standard parameters with label-free quantification (LFQ) and match between runs[60]. MS/MS spectra were matched against the UniProt Reference proteomes of *T. gondii* and Human (respectively Proteome ID UP000001529 and UP000005640) and 250 frequently observed contaminants as well as reversed sequences of all entries (MaxQuant contaminant database). Statistical analysis were done using Perseus on LFQ data[61].

Amino acid sequence alignments and phylogenetic analyses, cell and parasite culture, parasite cloning strategies, parasite transfections, parasite immunoblots, *T. gondii* plaque assays, *T. gondii* intracellular growth assay, *T. gondii* immunofluorescence-based induced egress assay, *T. gondii* conoid extrusion assay, *T. gondii* gliding assays, *T. gondii* attachment assay, Ciliata culture conditions, Ciliata biolistic transformation, generation of *Tetrahymena* knockout strain, Ciliata immunoblots, Ciliata immunofluorescence microscopy, statistical analysis, reagents and antibodies are found in Supplementary Methods.

Data availability

The datasets generated during and/or analysed during the current study are available from the corresponding author upon request.

References

1. Dubremetz, J. F. Rhoptries are major players in *Toxoplasma gondii* invasion and host cell interaction. *Cell Microbiol* **9**, 841–8 (2007).
2. Boothroyd, J. C. & Dubremetz, J. F. Kiss and spit: the dual roles of *Toxoplasma* rhoptries. *Nat Rev Microbiol* **6**, 79–88 (2008).
3. Carruthers, V. B. & Sibley, L. D. Sequential protein secretion from three distinct organelles of *Toxoplasma gondii* accompanies invasion of human fibroblasts. *Eur J Cell Biol* **73**, 114–23 (1997).
4. Frenal, K., Dubremetz, J. F., Lebrun, M. & Soldati-Favre, D. Gliding motility powers invasion and egress in Apicomplexa. *Nat Rev Microbiol* **15**, 645–660 (2017).
5. Besteiro, S., Dubremetz, J. F. & Lebrun, M. The moving junction of apicomplexan parasites: a key structure for invasion. *Cell Microbiol* **13**, 797–805 (2011).
6. Ito, D., Schureck, M. A. & Desai, S. A. An essential dual-function complex mediates erythrocyte invasion and channel-mediated nutrient uptake in malaria parasites. *Elife* **6**, (2017).
7. Counihan, N. A. *et al. Plasmodium falciparum* parasites deploy RhopH2 into the host erythrocyte to obtain nutrients, grow and replicate. *Elife* **6**, (2017).
8. Nguitragool, W. *et al.* Malaria parasite clag3 genes determine channel-mediated nutrient uptake by infected red blood cells. *Cell* **145**, 665–77 (2011).

9. Hakimi, M.-A., Olias, P. & Sibley, L. D. *Toxoplasma* Effectors Targeting Host Signaling and Transcription. *Clin. Microbiol. Rev.* **30**, 615–645 (2017).
10. Singh, S., Alam, M. M., Pal-Bhowmick, I., Brzostowski, J. A. & Chitnis, C. E. Distinct external signals trigger sequential release of apical organelles during erythrocyte invasion by malaria parasites. *PLoS Pathog* **6**, e1000746 (2010).
11. Kessler, H. *et al.* Microneme protein 8--a new essential invasion factor in *Toxoplasma gondii*. *J Cell Sci* **121**, 947–56 (2008).
12. Nichols, B. A., Chiappino, M. L. & O'Connor, G. R. Secretion from the rhoptries of *Toxoplasma gondii* during host-cell invasion. *J Ultrastruct Res* **83**, 85–98 (1983).
13. Coleman, B. I. *et al.* A Member of the Ferlin Calcium Sensor Family Is Essential for *Toxoplasma gondii* Rhoptry Secretion. *MBio* **9**, (2018).
14. Suarez, C. *et al.* A lipid-binding protein mediates rhoptry discharge and invasion in *Plasmodium falciparum* and *Toxoplasma gondii* parasites. *Nat Commun* **10**, 4041 (2019).
15. Tseng, T. T., Tyler, B. M. & Setubal, J. C. Protein secretion systems in bacterial-host associations, and their description in the Gene Ontology. *BMC Microbiol* **9 Suppl 1**, S2 (2009).
16. Gubbels, M.-J. & Duraisingh, M. T. Evolution of apicomplexan secretory organelles. *Int. J. Parasitol.* **42**, 1071–1081 (2012).
17. Plattner, H. Trichocysts-*Paramecium*'s Projectile-like Secretory Organelles: Reappraisal of their Biogenesis, Composition, Intracellular Transport, and Possible Functions. *J Eukaryot Microbiol* **64**, 106–133 (2017).
18. Plattner, H., Miller, F. & Bachmann, L. Membrane specializations in the form of regular membrane-to-membrane attachment sites in *Paramecium*. A correlated freeze-etching and ultrathin-sectioning analysis. *J Cell Sci* **13**, 687–719 (1973).

518 19. Knoll, G., Braun, C. & Plattner, H. Quenched flow analysis of exocytosis in *Paramecium*
519 cells: time course, changes in membrane structure, and calcium requirements revealed
520 after rapid mixing and rapid freezing of intact cells. *J Cell Biol* **113**, 1295–304 (1991).
521 20. Dubremetz, J. F. & Torpier, G. Freeze fracture study of the pellicle of an eimerian
522 sporozoite (Protozoa, Coccidia). *J Ultrastruct Res* **62**, 94–109 (1978).
523 21. Porchet, E. & Torpier, G. [Freeze fracture study of *Toxoplasma* and *Sarcocystis* infective
524 stages (author's transl)]. *Z Parasitenkd* **54**, 101–24 (1977).
525 22. Porchet-Hennere, E. & Nicolas, G. Are rhoptries of Coccidia really extrusomes? *J*
526 *Ultrastruct Res* **84**, 194–203 (1983).
527 23. Dubremetz, J. F. & Entzeroth, R. Exocytic events during cell invasion by Apicomplexa.
528 *Adv. Cell Mol. Biol. Membr. Membr. Traffic Protozoa Ed AM Tartakoff H Plattner* **2A**,
529 83–98 (1993).
530 24. Lefort-Tran, M., Aufderheide, K., Pouphile, M., Rossignol, M. & Beisson, J. Control of
531 exocytotic processes: cytological and physiological studies of trichocyst mutants in
532 *Paramecium tetraurelia*. *J Cell Biol* **88**, 301–11 (1981).
533 25. Beisson, J., Lefort-Tran, M., Pouphile, M., Rossignol, M. & Satir, B. Genetic analysis of
534 membrane differentiation in *Paramecium*. Freeze-fracture study of the trichocyst cycle in
535 wild-type and mutant strains. *J Cell Biol* **69**, 126–43 (1976).
536 26. Gogendeau, D., Keller, A. M., Yanagi, A., Cohen, J. & Koll, F. Nd6p, a novel protein
537 with RCC1-like domains involved in exocytosis in *Paramecium tetraurelia*. *Eukaryot*
538 *Cell* **4**, 2129–39 (2005).
539 27. Froissard, M., Keller, A. M. & Cohen, J. ND9P, a novel protein with armadillo-like
540 repeats involved in exocytosis: physiological studies using allelic mutants in
541 *Paramecium*. *Genetics* **157**, 611–20 (2001).

28. Skouri, F. & Cohen, J. Genetic approach to regulated exocytosis using functional complementation in *Paramecium*: identification of the ND7 gene required for membrane fusion. *Mol Biol Cell* **8**, 1063–71 (1997).
29. Froissard, M., Keller, A. M., Dedieu, J. C. & Cohen, J. Novel secretory vesicle proteins essential for membrane fusion display extracellular-matrix domains. *Traffic* **5**, 493–502 (2004).
30. Paredes-Santos, T. C., de Souza, W. & Attias, M. Dynamics and 3D organization of secretory organelles of *Toxoplasma gondii*. *J Struct Biol* **177**, 420–30 (2012).
31. Sidik, S. M. *et al.* A Genome-wide CRISPR Screen in *Toxoplasma* Identifies Essential Apicomplexan Genes. *Cell* **166**, 1423-1435 e12 (2016).
32. Long, S. *et al.* Calmodulin-like proteins localized to the conoid regulate motility and cell invasion by *Toxoplasma gondii*. *PLoS Pathog* **13**, e1006379 (2017).
33. Meissner, M., Schluter, D. & Soldati, D. Role of *Toxoplasma gondii* myosin A in powering parasite gliding and host cell invasion. *Science* **298**, 837–40 (2002).
34. Sheiner, L. *et al.* A systematic screen to discover and analyze apicoplast proteins identifies a conserved and essential protein import factor. *PLoS Pathog* **7**, e1002392 (2011).
35. Lamarque, M. H. *et al.* Plasticity and redundancy among AMA-RON pairs ensure host cell entry of *Toxoplasma* parasites. *Nat Commun* **5**, 4098 (2014).
36. Koshy, A. A. *et al. Toxoplasma* secreting Cre recombinase for analysis of host-parasite interactions. *Nat Methods* **7**, 307–9 (2010).
37. Collins, C. R. *et al.* Robust inducible Cre recombinase activity in the human malaria parasite *Plasmodium falciparum* enables efficient gene deletion within a single asexual erythrocytic growth cycle. *Mol Microbiol* **88**, 687–701 (2013).

566 38. Zhang, M. *et al.* Uncovering the essential genes of the human malaria parasite
567 *Plasmodium falciparum* by saturation mutagenesis. *Science* **360**, (2018).
568 39. Briguglio, J. S., Kumar, S. & Turkewitz, A. P. Lysosomal sorting receptors are essential
569 for secretory granule biogenesis in *Tetrahymena*. *J Cell Biol* **203**, 537–50 (2013).
570 40. Mueller, C. *et al.* The *Toxoplasma* protein ARO mediates the apical positioning of
571 rhoptry organelles, a prerequisite for host cell invasion. *Cell Host Microbe* **13**, 289–301
572 (2013).
573 41. Beisson, J., Cohen, J., Lefort-Tran, M., Pouphile, M. & Rossignol, M. Control of
574 membrane fusion in exocytosis. Physiological studies on a *Paramecium* mutant blocked
575 in the final step of the trichocyst extrusion process. *J Cell Biol* **85**, 213–27 (1980).
576 42. Bonnemain, H., Gulik-Krzywicki, T., Grandchamp, C. & Cohen, J. Interactions between
577 genes involved in exocytotic membrane fusion in *Paramecium*. *Genetics* **130**, 461–70
578 (1992).
579 43. Varghese, T. Fine structure of the endogenous stages of *Eimeria labbeana*. I. The first
580 generation merozoites. *J Protozool* **22**, 66–71 (1975).
581 44. Sheffield, H. G. Electron microscope study of the proliferative form of *Besnoitia*
582 *jellisoni*. *J Parasitol* **52**, 583–94 (1966).
583 45. Perkins, F. O. Zoospores of the Oyster Pathogen, *Dermocystidium marinum*. I. Fine
584 Structure of the Conoid and Other Sporozoan-Like Organelles. *J. Parasitol.* **62**, 959–974
585 (1976).
586 46. El Hajj, H. *et al.* Molecular signals in the trafficking of *Toxoplasma gondii* protein MIC3
587 to the micronemes. *Eukaryot Cell* **7**, 1019–28 (2008).
588 47. Collins, C. R., Withers-Martinez, C., Hackett, F. & Blackman, M. J. An inhibitory
589 antibody blocks interactions between components of the malarial invasion machinery.
590 *PLoS Pathog* **5**, e1000273 (2009).

591 48. Burghaus, P. A. & Holder, A. A. Expression of the 19-kilodalton carboxy-terminal
592 fragment of the *Plasmodium falciparum* merozoite surface protein-1 in *Escherichia coli*
593 as a correctly folded protein. *Mol Biochem Parasitol* **64**, 165–9 (1994).
594 49. Douki, J. B. *et al.* Adhesion of normal and *Plasmodium falciparum* ring-infected
595 erythrocytes to endothelial cells and the placenta involves the rhoptry-derived ring
596 surface protein-2. *Blood* **101**, 5025–32 (2003).
597 50. Schindelin, J. *et al.* Fiji: an open-source platform for biological-image analysis. *Nat*
598 *Methods* **9**, 676–82 (2012).
599 51. Cerede, O. *et al.* Synergistic role of micronemal proteins in *Toxoplasma gondii* virulence.
600 *J Exp Med* **201**, 453–63 (2005).
601 52. Branton, D. *et al.* Freeze-etching nomenclature. *Science* **190**, 54–6 (1975).
602 53. Knuepfer, E., Napiorkowska, M., van Ooij, C. & Holder, A. A. Generating conditional
603 gene knockouts in *Plasmodium* - a toolkit to produce stable DiCre recombinase-
604 expressing parasite lines using CRISPR/Cas9. *Sci Rep* **7**, 3881 (2017).
605 54. Iancu, C. V. *et al.* Electron cryotomography sample preparation using the Vitrobot. *Nat.*
606 *Protoc.* **1**, 2813–2819 (2006).
607 55. Mastronarde, D. N. Automated electron microscope tomography using robust prediction
608 of specimen movements. *J Struct Biol* **152**, 36–51 (2005).
609 56. Kremer, J. R., Mastronarde, D. N. & McIntosh, J. R. Computer visualization of three-
610 dimensional image data using IMOD. *J Struct Biol* **116**, 71–6 (1996).
611 57. Lebrun, M. *et al.* The rhoptry neck protein RON4 relocalizes at the moving junction
612 during *Toxoplasma gondii* invasion. *Cell Microbiol* **7**, 1823–33 (2005).
613 58. Skorupa, A. *et al.* Angiogenin induces modifications in the astrocyte secretome:
614 relevance to amyotrophic lateral sclerosis. *J Proteomics* **91**, 274–85 (2013).

59. Cox, J. & Mann, M. MaxQuant enables high peptide identification rates, individualized p.p.b.-range mass accuracies and proteome-wide protein quantification. *Nat Biotechnol* **26**, 1367–72 (2008).
60. Cox, J. *et al.* Andromeda: a peptide search engine integrated into the MaxQuant environment. *J Proteome Res* **10**, 1794–805 (2011).
61. Tyanova, S. *et al.* The Perseus computational platform for comprehensive analysis of (prote)omics data. *Nat Methods* **13**, 731–40 (2016).
62. Wilson, D., Madera, M., Vogel, C., Chothia, C. & Gough, J. The SUPERFAMILY database in 2007: families and functions. *Nucleic Acids Res* **35**, D308-13 (2007).
63. Hadjebi, O., Casas-Terradellas, E., Garcia-Gonzalo, F. R. & Rosa, J. L. The RCC1 superfamily: from genes, to function, to disease. *Biochim Biophys Acta* **1783**, 1467–79 (2008).

Acknowledgements

We thank Sebastian Lourido for the pU6-Universal plasmid, Artur Scherf for anti-*Pf*RAP2 antibodies, Soldati-Favre for providing us the anti-ARO antibodies and *TgARO*-iKD strain; Michael Blackman for antibodies (anti-PfAMA1 and anti-*Pf*MSP1), pDC2-Cas9-hDHFRyFCU plasmid, and *p230p* DiCre strain; John Boothroyd for mAb CCL2 anti-*Tg*AMA1; Ross Waller for RNG1-GFP plasmid; Anita Koshy for the toxofilin-Cre plasmid and Helen Blau's lab for the Cre reporter DSred cell line. We thank Oliver Billker for providing us with Compound 2. We thank Veronique Richard and Frank Godiard for their technical assistance on the electron microscopy service of the University of Montpellier. We are also grateful to Elodie Jublanc and the imaging facility MRI at the University of Montpellier, part of the national infrastructure France-BioImaging supported by the French

National Research Agency (ANR-10-INBS-04, «Investments for the future»), and Christophe Duperray of the MRI-Cytometry at the Institute for Regenerative Medicine and Biotherapy for their assistance and technical support. We would like to thank Julien Marcetteau for the graphical design of Fig. 1b and Fig. 4. We acknowledge the use of instruments at the Electron Microscopy Resource Laboratory and the Beckman Center for Cryo-Electron Microscopy at the University of Pennsylvania. Dr Maryse Lebrun is an INSERM researcher. This work was supported by the Laboratoire d'Excellence (LabEx) (ParaFrap ANR-11-LABX-0024), the ANR (ANR-16-CE15-0010-01), and the Fondation pour la Recherche Medicale (Equipe FRM DEQ20170336725) to M.L.; by the FACCTS (France and Chicago Collaborating in the Sciences) to A.P.T and M.L. ;by NIH GM105783 to A.P.T. ;by a David and Lucile Packard Fellowship for Science and Engineering (2019-69645) to Y.-W.C and by EMBO fellowship number ALTF 58-2018 to A.N.G..

Author contributions

E.A. performed most of the work on *Toxoplasma*. M.M.C generated the *Plasmodium* data and completed the work on *Toxoplasma* during revision. A.G. performed the phylogenetic analyses. E.A. D.S and R. N. generated the *T. thermophila* data. C.S. generated the donor plasmid for *Pfnd9*-iKO. A.N.G., N.D.S.P., R.N. and M.M. contributed to *Toxoplasma* phenotypic analyses. D.M.P.V. performed the IP analyses. S. U. performed the mass spectrometry analyses. E.A., L.B-S and J.F.D. performed electron-microscopy. E. A., P.R.F and J.F.D. performed the freeze fracture analyses. S.K.M. and Y.-W.C. performed the cryo-ET. A.N.G. and S.K.M. prepared the samples for cryo-ET. M.L. designed the study with the support of E.A. M.L. supervised the research. E.A. and M.L. wrote the paper with editorial support from M.M.C., A.P.T., D.S., A.N.G., S.K.M., Y.-W.C. and B. S. The data are included in the main manuscript and in the supplementary materials.

Competing interests

The authors declare no competing financial interests.

Materials and Correspondence

Correspondence and requests for materials should be addressed to M.L.

Supplementary Information is available for this paper.

Fig. 1 | Rhoptry secretion is dependent on rosette formation.

a, Immunofluorescence assay (IFA) of control untagged line and endogenously HA_3-tagged *Tg*Nd6 and HA_3-tagged *Tg*Nd9 tachyzoites. The green arrow points to *Tg*Nd6 apical puncta. ARO is a marker for rhoptries. Shown are maximum intensity projections of confocal z-stacks of fixed parasites. **b**, Super-resolution microscopy of the apical dot of *Tg*Nd6. Schematic of apical end of tachyzoite. Maximum intensity projections of z-stacks of *Tg*Nd6-HA_3 parasites transiently expressing RNG1_GFP (top) and of *Tg*Nd6-HA_3 parasites expressing centrin 2 (CEN2)-Ty_2 (bottom). The protein RNG1_GFP marks the apical polar ring (APR) and CEN2_Ty marks pre-conoidal rings (PCR). Higher magnifications show that *Tg*Nd6-HA_3 (red arrow) localizes above the apical polar ring (green arrow) and co-localizes partially with CEN2. DIC: differential interference contrast. **c**, Immunogold labelling of *Tg*Nd6-HA_3. Right panel shows *Tg*Nd6-HA_3 on the AV. Insert panel: higher magnification of the AV. Micronemes (m) and rhoptries (Rh) are visible in transverse section of the conoid (Co). **d,** Quantification of invasion after depletion of *Tg*Nd6 and *Tg*Nd9. Mean ± SD of n=3 independent experiments. **e**, Immunoblot showing microneme secretion assessed by the release of proteolytically cleaved AMA1 (arrow=processed/secreted *Tg*AMA1) in *Tgnd6*-

690 iKD ± IAA 24 h (left) and *Tgnd9*-iKD ± ATC 72 h (right). P = pellet, Sup = supernatant, Sup
691 ind = propanolol-induced supernatant. GRA3, loading control. **f**, Rhoptry secretion assay by
692 Secreted Cre, epitope-tagged (SeCrEt). Rhoptry secretion quantification of *Tgnd6*-iKD (left)
693 ± IAA and *Tgnd9-i*KD (right) ± ATC. Mean ± SD of n=3 independent experiments. **g**, Left:
694 Freeze-fracture electron microscopy of a *T. gondii* tachyzoite (P face) showing a rosette of
695 intramembranous particles (white arrow) at the middle of the apex. Middle: Higher
696 magnification of the left panel. The white arrowheads point to the eight IMPs of the rosette.
697 Right: Quantification of rosettes of IMPs in *Tgnd9*-iKD ± ATc 72 h and *Tgnd6*-iKD ± IAA
698 24 h using freeze fracture. (**d, f**) Unpaired two tail student's *t* test: **** *p*-value < 0.0001,
699 *** *p*-value < 0.001, ** *p*-value < 0.01, * *p*-value < 0.05.

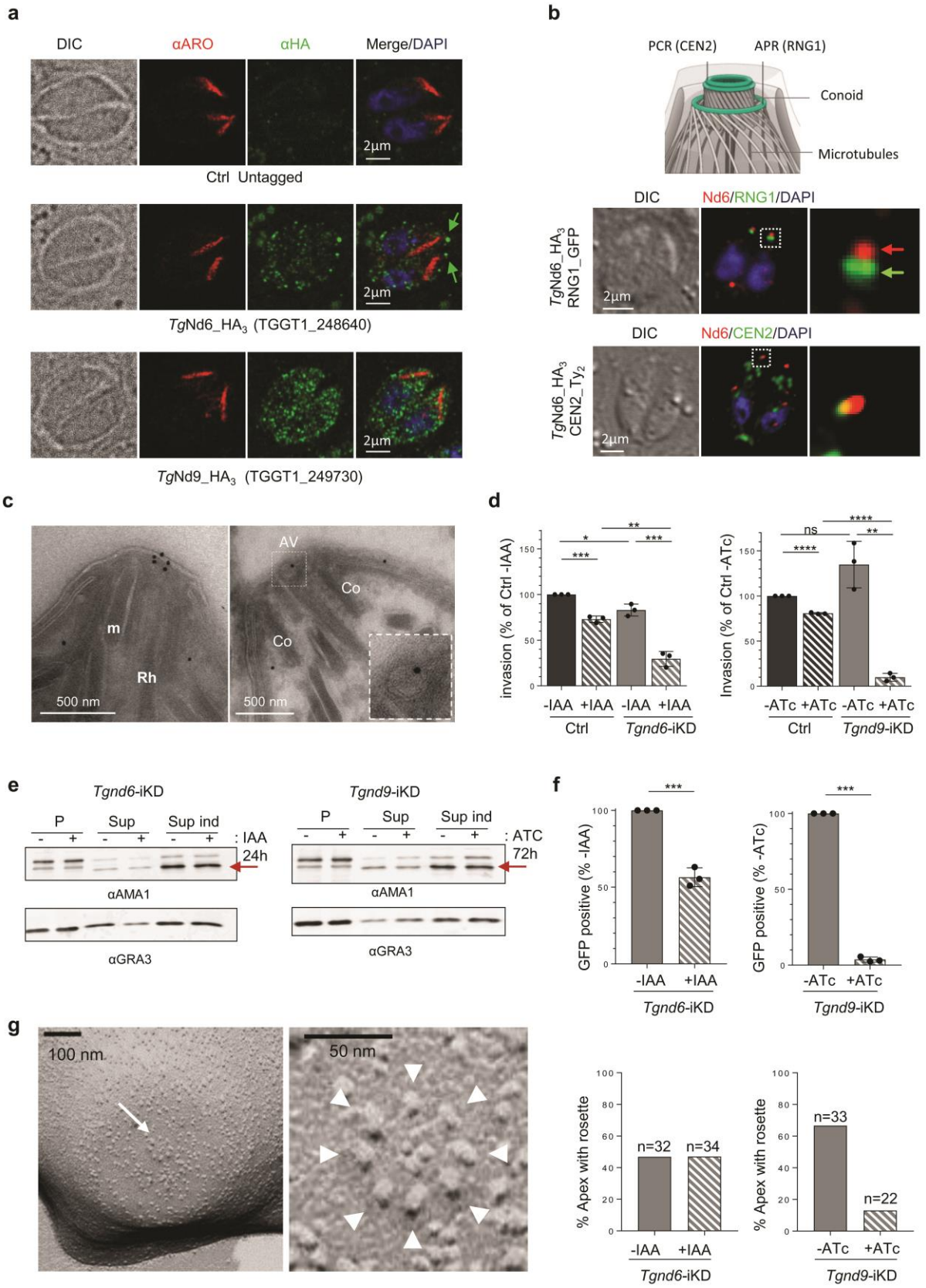
a
DIC
αARO
αHA
Merge/DAPI
2µm
Ctrl Untagged
TgNd6_HA3 (TGGT1_248640)
TgNd9_HA3 (TGGT1_249730)
b
PCR (CEN2)
APR (RNG1)
Conoid
Microtubules
DIC
Nd6/RNG1/DAPI
TgNd6_HA3 RNG1_GFP
Nd6/CEN2/DAPI
TgNd6_HA3 CEN2_Ty2
c
m
Rh
AV
Co
500 nm
d
invasion (% of Ctrl -IAA)
-IAA +IAA -IAA +IAA
Ctrl
Tgnd6-iKD
Invasion (% of Ctrl -ATc)
-ATc +ATc -ATc +ATc
Tgnd9-iKD
e
Tgnd6-iKD
Tgnd9-iKD
P
Sup
Sup ind
: IAA 24h
: ATC 72h
αAMA1
αGRA3
f
GFP positive (% -IAA)
GFP positive (% -ATc)
g
100 nm
50 nm
% Apex with rosette
n=32
n=34
n=33
n=22

Fig. 2 | *Pf*Nd9 is essential for rhoptry secretion in *P. falciparum*.

a, Freeze-fracture electron microscopy of a *P. falciparum* merozoite (P face) showing a rosette of intramembranous particles (white arrow). Higher magnification at the bottom. Bar is 100 nm. **b**, Growth curves (parasitaemias) of *p230p* DiCre (Ctrl) and *Pfnd9*-iKO mutant ± rapamycin shows that *Pf*Nd9-depleted parasites have a growth defect. On the right: Giemsa staining of the growth experiment illustrating development and reinvasion of *p230p* DiCre (Ctrl) and *Pfnd9*-iKO asexual parasites (along 2 cycles) ± rapamycin treatment. **c,** Quantification of egress of *Pfnd9*-iKO ± rapamycin schizonts. Data collected from 8 movies of *Pfnd9*-iKO ± rapamycin. **d**, Left: IFA illustrating AMA1 protein stored in micronemes (top) or secreted and translocated at the surface of the parasite prior to egress (bottom). . **e**, Quantification of rhoptry secretion events in *Pfnd9*-iKO ± rapamycin-treated schizonts using anti-*Pf*RAP2 antibodies to visualise rhoptry secretion events ('spits' of RAP2 exported into the RBC). (e) Unpaired two tail student's *t* test: **** *p*-value < 0.0001.

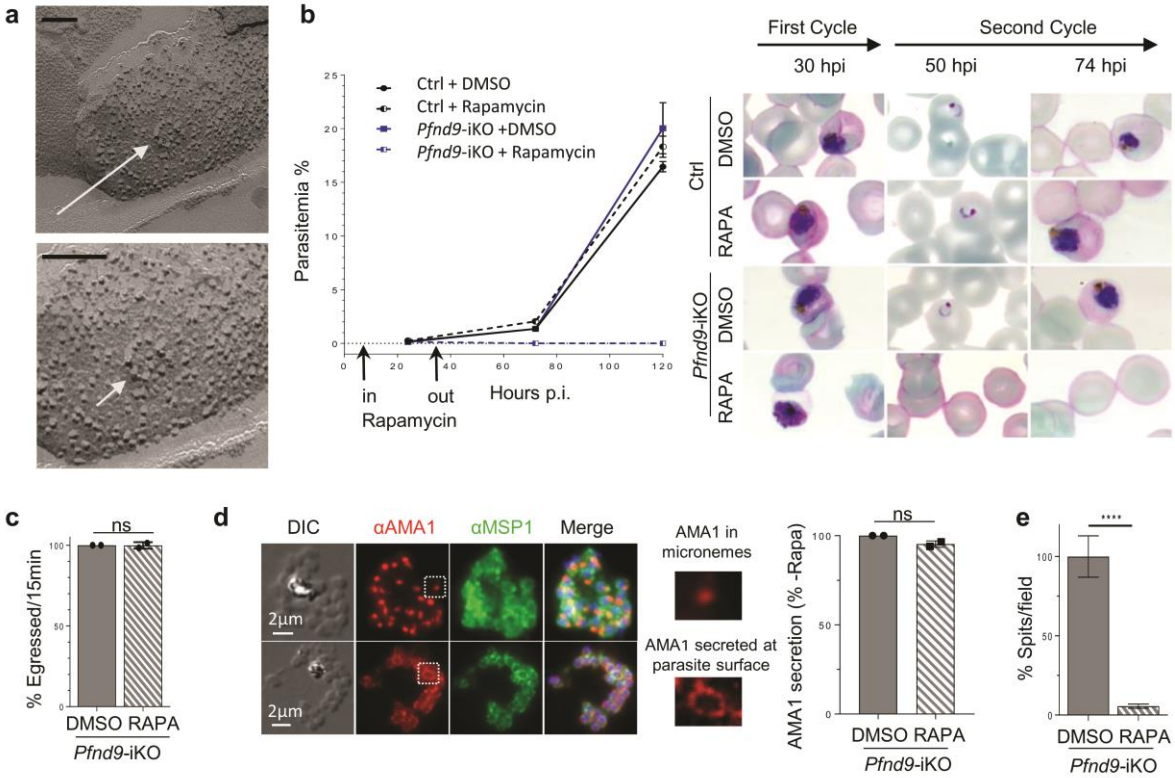

Fig. 3 | Nd6 and Nd9 are part of an Alveolata complex essential for organelle secretion in *T. gondii* (Apicomplexa) and *T. thermophila* (Ciliata)

a, Mass spectrometry analysis of immuno-isolated *Tg*Nd9-HA_3. Left: Volcano Plot of proteins differentially enriched in *Tg*Nd9 vs control IP. This plot presents the fold change (Difference) and significance (-Log p) obtained from a t-test of three independent IPs using LFQ intensity values. Right: Schematic representation of *Tg*Nd proteins using SUPERFAMILY[62]. RCC1: regulator of chromosome condensation 1-like domains (RLDs), a versatile domain that performs many different functions, including guanine nucleotide exchange on small GTP-binding proteins[63]. LRR: Leucine Rich Repeat domain. ARM: Armadillo Repeat domain. C2: lipid-calcium binding domain. **b**, Immunofluorescence (IF) of endogenously HA_3-tagged *Tg*NdP1 and *Tg*NdP2 tachyzoites. The white arrow points to *Tg*NdP1 apical dots of two adjacent parasites, which are magnified on the right. ARO: rhoptry marker. DAPI: DNA marker. DIC: differential interference contrast. **c,** Quantification of invasion after depletion of *Tg*NdP1 (left; using ATc) and *Tg*NdP2 (right; using IAA) along with negative control strains. Mean ± SD of n=3 independent experiments. **d,** Rhoptry secretion quantification of *TgndP1*-iKD (left) ± ATc and *TgndP2*-iKD (right) ± IAA. Mean ± SD of n=3 independent experiments. **e**, Quantification of rosettes of IMPs in *TgndP1*-iKD ± ATc 72 h and in *TgndP2*-iKD ± IAA 24 h using freeze-fracture. **f,** Quantification of mucocyst exocytosis by dibucaine assay. Data collected from three experiments. (**c-f**) Unpaired two tail student's *t* test: **** *p*-value < 0.0001, *** *p*-value < 0.001, ** *p*-value < 0.01, * *p*-value < 0.05.

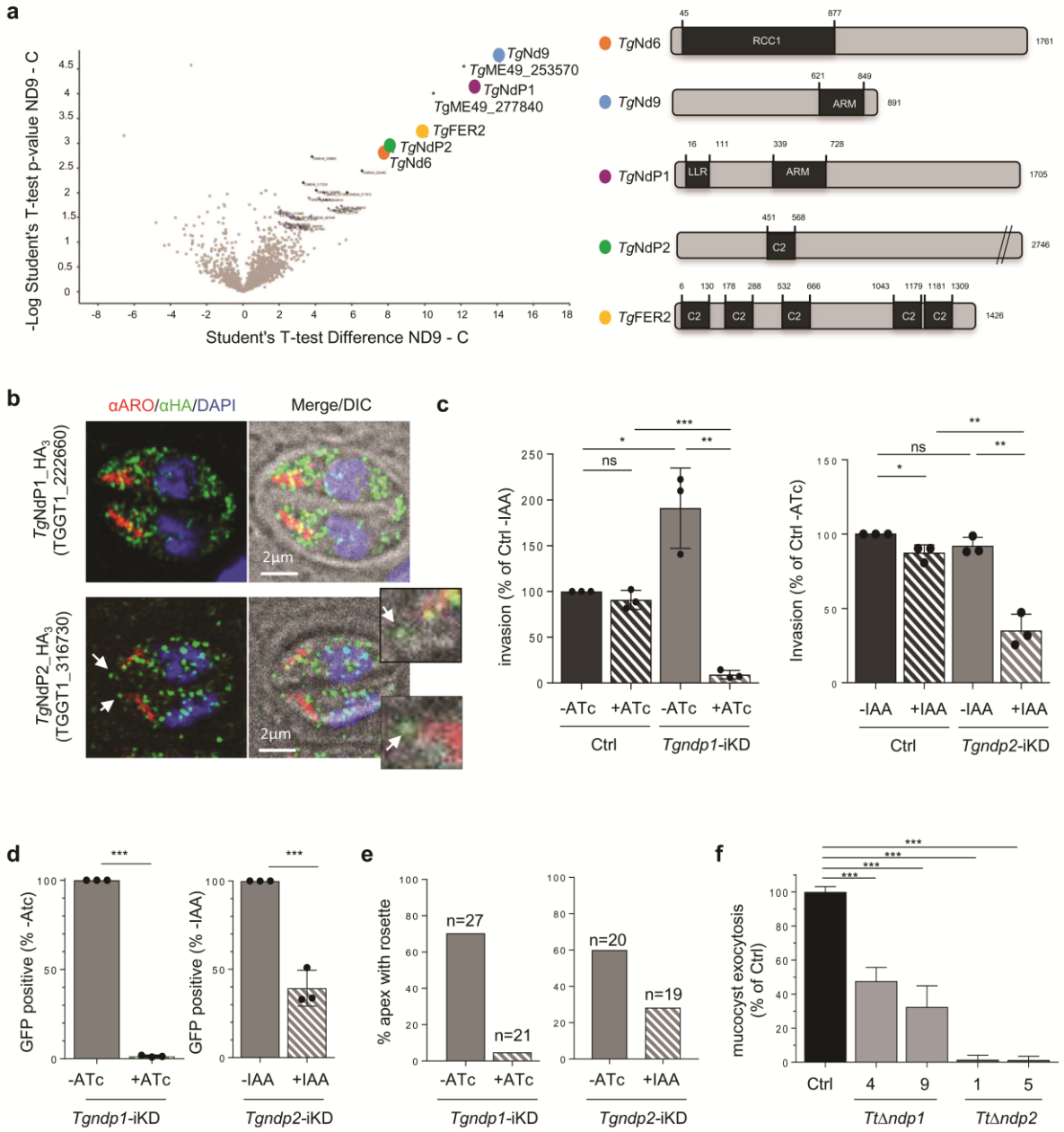
a
-Log Student's T-test p-value ND9 - C
Student's T-test Difference ND9 - C
TgNd9
TgME49_253570
TgNdP1
TgME49_277840
TgFER2
TgNdP2
TgNd6
TgNd6
RCC1
TgNd9
ARM
TgNdP1
LLR
ARM
TgNdP2
C2
TgFER2
C2
b
αARO/αHA/DAPI
Merge/DIC
TgNdP1_HA3 (TGGT1_222660)
TgNdP2_HA3 (TGGT1_316730)
2µm
c
invasion (% of Ctrl -IAA)
Invasion (% of Ctrl -ATc)
-ATc
+ATc
-IAA
+IAA
Ctrl
Tgndp1-iKD
Tgndp2-iKD
d
GFP positive (% -Atc)
GFP positive (% -IAA)
e
% apex with rosette
n=27
n=21
n=20
n=19
f
mucocyst exocytosis (% of Ctrl)
Ctrl
4
9
1
5
TtΔndp1
TtΔndp2

739

740

741

Fig. 4 | The rhoptry secretion machinery includes the apical vesicle and the rosette

a, A slice through a tomogram showing a side view of the apical complex – conoid (brown), pre-conoidal apical rings (PCR; gray; two in number), micronemes (yellow), plasma membrane (PM; light blue) and the rhoptry secretion system consisting of the rosette (dark blue), apical vesicle (AV; magenta), rhoptry (orange) and rhoptry tip density (cyan). Original image (right) is annotated with color overlays (left). **b,** Left: magnified image of the boxed region in (a) showing the connections between the rhoptry, rhoptry tip density, AV, rosette and the PM. The rhoptry tip is 9 nm distant from the AV. Right: a pair of 3-dimensional segmentations from the data on the left. The PM is rendered transparent in one of these segmentations to see the rosette. **c,** Magnified image of the boxed region in (b) showing the side view of the rosette. The AV is 14 nm distant from the PM. **d)** Top view of the rosette from a horizontal tomogram section perpendicular to the plane in (c), showing an 8-fold rotational symmetry and a diameter of ~67 nm. **e)** AV connected with the PM via a rosette in the absence of docked rhoptry. All measurements are made in 3D. Images in (b-e) are computationally filtered to boost contrast (see Methods). The images in (c) and (d) are from two different cells oriented differently on the EM grid resulting in better resolved side view and top view, respectively. **f,** Quantification of apical rosettes in *TgARO*-iKD mutants ± ATc 72 h. **g,** Left: Ultrastructure of wild type (RH strain type I) tachyzoites with the AV positioned beneath the plasma membrane, and above the tip of the rhoptry neck. Right: In *TgARO*-iKD ATc-treated tachyzoites (72 h), the AV is still properly positioned at the apex (presumably under the rosette), while rhoptries are not docked on the AV. Inset shows a magnification of the vesicles. co: conoid; m: micronemes; Rh: rhoptry; APR: apical polar ring; PCR: pre-conoidal rings; AV: apical vesicle; ICM: pair of intraconoidal microtubules. **h,** Schematic of similarities and differences of the exocytic machinery between Ciliata and

767 Apicomplexa. Exocytosis in Alveolata (Ciliata, Dinoflagellata and Apicomplexa) is outlined
768 by the presence of a rosette of particles embedded in the outer membrane, defining the site of
769 exocytosis. In Ciliata, organelles discharge can have a defensive or predatory function.
770 Rhoptry exocytosis in Apicomplexa is one of the critical steps of host cell invasion and
771 therefore fundamental for parasitism. In Apicomplexa, but not in Ciliata, an apical vesicle
772 (AV) of unknown function is present between the tip of the rhoptry and the plasmalemma,
773 plausibly involved in the injection of rhoptry proteins into the host cell. PM, plasma
774 membrane; PVM, parasitophorous vacuole membrane; AS, alveolar sac [in Ciliata], which is
775 homologous to the IMC (inner membrane complex) of Apicomplexa.

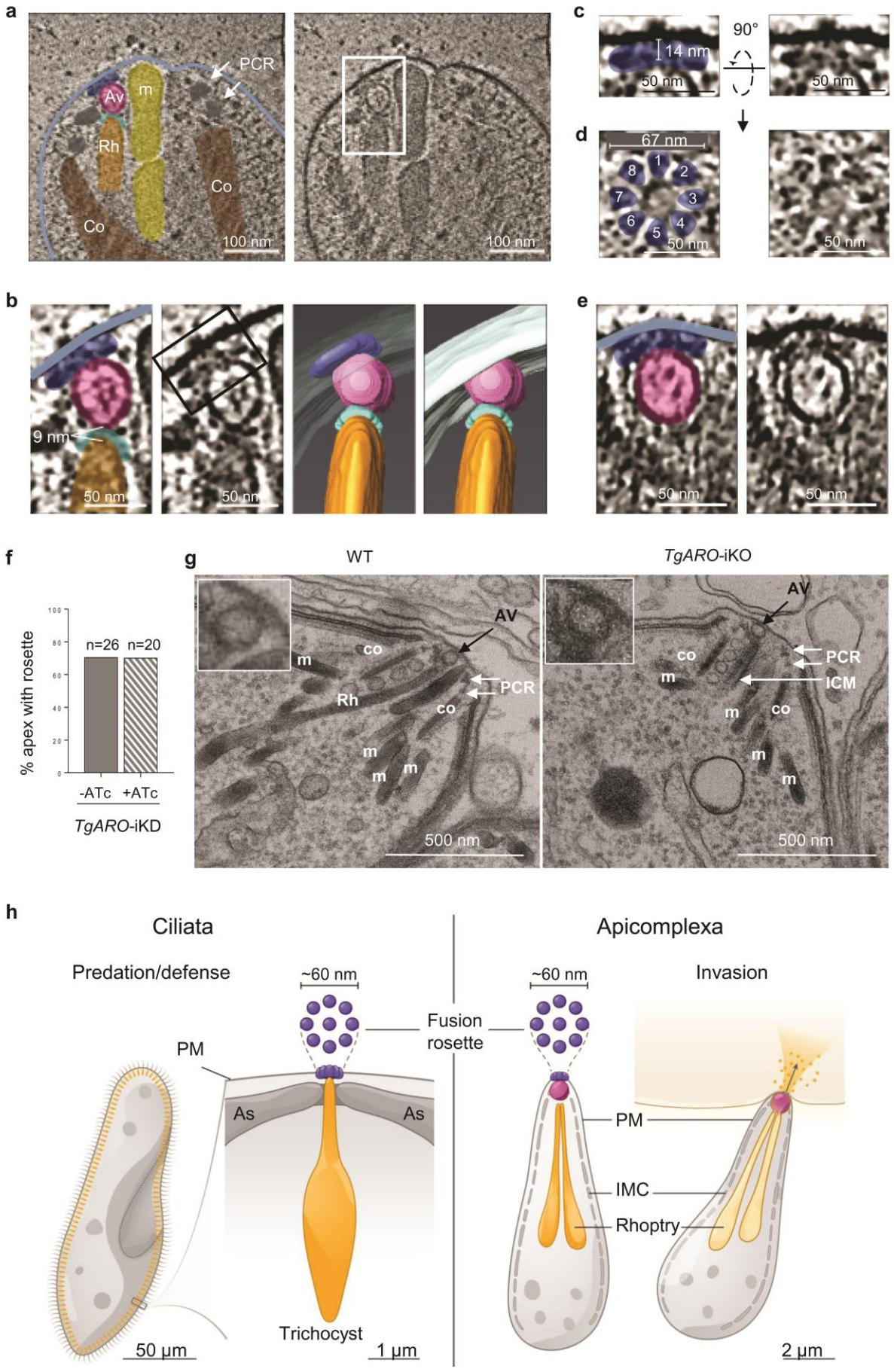
a
PCR
Av
m
Rh
Co
Co
100 nm
100 nm
c
14 nm
50 nm
90°
50 nm
d
67 nm
1
2
3
4
5
6
7
8
50 nm
50 nm
b
9 nm
50 nm
50 nm
e
50 nm
50 nm
f
% apex with rosette
n=26
n=20
-ATc
+ATc
TgARO-iKD
g
WT
TgARO-iKO
AV
PCR
co
m
Rh
ICM
500 nm
500 nm
h
Ciliata
Apicomplexa
Predation/defense
Invasion
~60 nm
~60 nm
Fusion rosette
PM
As
As
PM
IMC
Rhoptry
Trichocyst
50 µm
1 µm
2 µm

776